Available online at www.sciencedirect.com

SciVerse ScienceDirect

Physics Procedia 37 (2012) 1113 – 1121

Physics Procedia

TIPP 2011 - Technology and Instrumentation in Particle Physics 2011

Neutron to Gamma Pulse Shape Discrimination in Liquid Argon Detectors with High Quantum Efficiency Photomultiplier Tubes

R. Acciarri[a], N. Canci[b,*], F. Cavanna[a,1], P. Kryczynski[c], L. Pandola[b], E. Segreto[b], A.M. Szelc[a,c,1]

[a] *Università dell'Aquila e INFN, L'Aquila, Italy*
[b] *INFN - Laboratori Nazionali del Gran Sasso, Assergi, Italy*
[c] *IFJ PAN, Krakow, Poland*

Abstract

A high Light Yield Liquid Argon chamber has been radiated with an Am/Be source for signal-to-background separation level characterization in a Dark Matter Liquid Argon based detector. Apart from the standard nuclear recoil and electron events, from neutron elastic interactions and gamma conversions respectively, an intermediate population has been observed which is attributed to inelastic neutron scatters on Argon nuclei producing Argon recoil and simultaneous gammas from nuclear de-excitation. Taking account of these events results in a better determination of the recoil-like to electron-like separation based on the shape of the scintillation pulse. The results of this recent study as well as from a previous study with a chamber with a lower Light Yield are presented.

Keywords: Liquid Argon, Noble Liquid detectors, Cryogenic Detectors, Dark Matter search, Pulse Shape Discrimination, Particle identification

1. Introduction

Searching for Dark Matter in the form of WIMPs is of primary interest in the present astroparticle physics scenario. Direct detection of Dark Matter using liquified noble gases (Neon, Argon and Xenon) as the target medium is one of the most promising lines of development in experimental technology.
Argon in particular, due to its high scintillation photon yield, ease of purification and high abundance at reasonable cost, represents a suitable medium and the feasibility of Ar-based detectors has been firmly proven by the R&D study of the WArP collaboration [1]. Because Dark Matter particles are so elusive, any experiment aiming to detect them must precisely understand and discriminate background events.
In Liquid Argon (LAr) this can be done using the potential offered by its scintillation characteristics which

*Corresponding author.
Email address: nicola.canci@lngs.infn.it (N. Canci)
[1] Currently at Yale University - New Haven, Connecticut, USA.

1875-3892 © 2012 Published by Elsevier B.V. Selection and/or peer review under responsibility of the organizing committee for TIPP 11. Open access under CC BY-NC-ND license. doi:10.1016/j.phpro.2012.03.732

allow the implementation of Pulse Shape Discrimination (PSD) methods in order to maximize the background rejection. Therefore the choice, the study and the optimization of such techniques represents an important step on the way to realize a successful experiment.

2. Scintillation Light in Liquid Argon

Ionization in liquid Argon is accompanied by the emission of scintillation light. Charged particles interacting in LAr create free electrons (e^-) and excited Ar molecular states (Ar_2^*) which produce scintillation radiation through de-excitation processes [2]:

$$Ar_2^* \rightarrow 2\,Ar + \gamma \tag{1}$$

Therefore, free electron separation and light emission are the two features that characterize the use of LAr as active medium [3]. The two processes are complementary and their relative weight depends on the strength of the electric field (EF) applied to the active LAr volume [3]. The free electron yield (from ionization) rises with the field value while the photon yield (from scintillation) decreases[2].
The light emission is characterized by a rather narrow intrinsic spectrum ($\lambda \simeq 128$ nm with $\sigma_\lambda \simeq 3$ nm) in the extreme ultra-violet region (Vacuum-UV, VUV) [6] [7] and by a two-component exponential decaying (fast from the Singlet and slow from the Triplet excimer state decay), with lifetimes $\tau_S = 4 \div 7$ ns and $\tau_T = 1.3 \div 1.6\,\mu$s respectively [6] [8] [9]. In addition to these fast and slow components, an *intermediate* component (with decay time around 40÷60 ns) has been also sometime reported in literature [9] [10] [11], the origin of which was never definitively understood.
The relative amplitude ratio of the fast to the slow component in case of a *mip* is reported to be $A_S/A_T = 0.3$ (i.e. $A_S = 23\%$ and $A_T = 77\%$ respectively) [9]; while for heavily ionizing particles the intensity ratio increases (e.g. $A_S/A_T = 1.3$ for α-particles and $A_S/A_T = 3$ for nuclear recoils [12]).
This wide separation is an important feature of the scintillation signals in LAr, leading to define robust Pulse Shape Discrimination criteria suitable for particle identification.

3. Pulse Shape Discrimination in LAr

Pulse Shape Discrimination is a background discrimination and rejection technique; in LAr detectors the different ratio of fast to slow component for diverse particles results in two distinct rise-times of signals produced by the recoil-like events (neutron or WIMP interactions) and electron-like events (electron and gamma interactions), as shown in Fig. 1.
The very different shape of the two pulses is characteristic of the Argon scintillation light emission. This feature is on of the main discrimination methods, which can be applied for signal (Ar-recoil) to background (e-recoil) separation in LAr based detector.

As indicated before, PSD in LAr can be explained in terms of the properties of de-excitation of the excited Ar_2^* dimers . In fact, the time evolution of the LAr scintillation light emission depends on the two very different decay times of the Singlet and the Triplet dimer states respectively to the ground state and their relative abundance in ionization process induced by different particles.

4. First PSD studies

Within the WArP R&D phase, early dedicated studies have been performed in 2007-2009 with the aim of optimizing the PSD of β and γ background. For this task, a single phase (no electric fields applied to the active volume) 4 liter LAr detector equipped with seven 2" PMTs (ETL - D749U) has been used (photo-cathode coverage $\sim 12\%$); signals from PMTs have been directly acquired by a waveform digitizer

[2]For a minimum ionizing particle (*mip*) at low fields (e.g. 0.5 kV/cm) the free electron yield is $Y_{ion} \sim 2.9\times10^4$ e^-/MeV [4]. At the same EF the photon yield is also high ($Y_{ph} \sim 2.4\times10^4$ γ/MeV) [5]. The photon yield is maximum at null field, $Y_{ph}(mip) \simeq 4\times10^4$ γ/MeV.

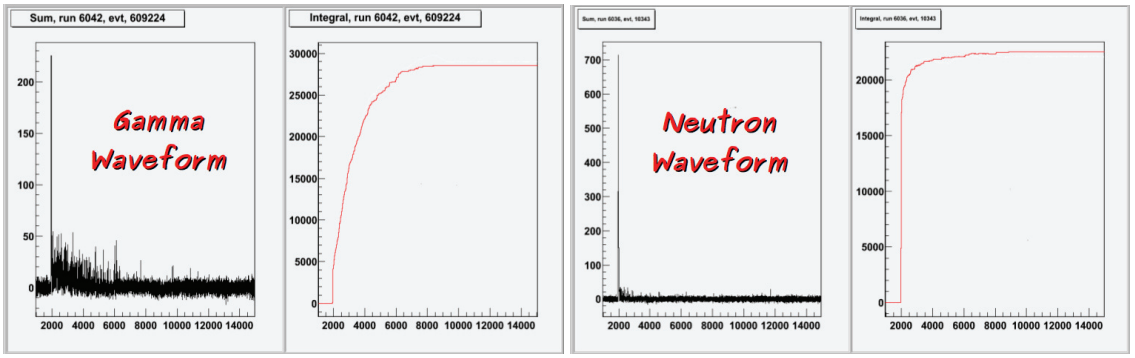

Fig. 1. *Gamma-like event [Left] and Neutron-like event [Right], shown as sum of the raw waveforms collected by seven PMTs and event integrals, calculated from 100 ns before the trigger to 7 μs after the trigger.*

(Acqiris-U1080A) and then processed off-line [13].
Two radioactive sources have been used during the data acquisition: a ^{133}Ba gamma source and a Am/Be neutron (and gamma) source.
Events collected with the ^{133}Ba source have been used to determine the Light Yield (LY) of the system (the energy spectrum obtained for each run was compared with a MonteCarlo simulation): the light response of the apparatus was stable during the test and a LY estimation of 1.52 ± 0.05 phe/keV has been obtained.
The Am/Be source, inducing both nuclear-recoil (from neutron interactions) and electron-recoil (from γ conversion through photoelectric absorption or Compton scattering) events in the detector, has been used to study the discrimination power of different PSD methods.
Different PSD techniques and their discrimination power have been applied to the whole of the collected data ($\simeq 8.56 \cdot 10^6$ events), optimized and compared with each other: the *F-prompt* method was found to be the most appropriate among those taken into consideration [13].

4.1. F-prompt discrimination method

The *F-prompt* (F_p) method represents a fast and easy way to perform pulse shape discrimination of gamma-like and neutron-like events.
Taking $V(t)$ as the sum of the waveforms collected for a given ionization event, the F_p parameter associated to that event is defined as:

$$F_p = \frac{\int_{T_0}^{T_{F_p}} V(t)dt}{\int_{T_0} V(t)dt} = \frac{S_F}{S_1} \tag{2}$$

where S_1 is the total integral of the event pulse $V(t)$ and S_F (Fast signal integral) represents the integral of the first part of the signal, up to an integration time T_{F_p} after the trigger T_0. The integration time T_{Fp} of fast integral S_F has been optimized[3] driven by the aim of maximizing the separation between nuclear recoil and electron recoil in the F_p distributions and the best value was found to be 120 ns [13].

4.2. Data analysis of the first run

The *F-prompt* method was implemented to separate electron recoils from nuclear recoils. In Fig. 2 both the F_p distribution for one of the runs belonging to the analysis data sample [Left] and a scatter plot of F_p versus event energy (in photo-electron units) [Right] are shown. Two populations are clearly visible in the

[3]Considering a fast decay time of few ns and a slow decay time $\sim \mu$s for LAr scintillation light emission $T_{F_p} = 10 \div 20$ ns can be expected; a set value of $T_{F_p} \sim 120$ ns can be ascribed to the presence of an intermediate decay component with $\tau_i \sim 60$ ns in the LAr scintillation light. Taking into account an interval in which 80< T_{F_p} <150 ns, the choice of $T_{F_p} \sim 120$ ns was obtained using two different and indipendent methods leading to the same best result: the first based on a direct analysis of the F_p distributions, the latter on the analysis of the average waveforms realized from electron recoil and nuclear recoil events [13].

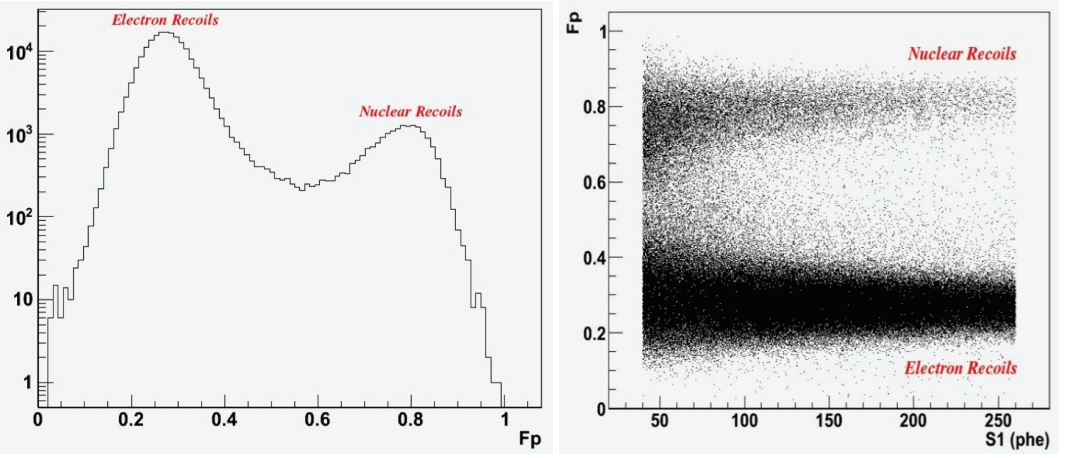

Fig. 2. F_p distribution [Left] and a scatter plot of F_p versus event energy (phe units) [Right].

plots: the first, clustered at higher F_p values, corresponds to nuclear recoil events, the latter, at lower F_p values, is due to electron recoil events. In the middle, a third population of events with $F_{p_\gamma} < F_{p_i} < F_{p_n}$ has been detected. We ascribed this intermediate population to the result of inelastic scattering of neutron on Ar nuclei. The origin of the inelastic events can be better deduced when looking at the energy spectrum of the Am/Be source used in the data taking, which emits a large part of the neutrons in the $2 \div 6$ MeV energy range (Fig. 3 [Left]) [14]; comparing it with the cross-section spectrum for different neutron interactions on the ^{40}Ar nuclei, one can observe that the inelastic scattering starts to be important at these energies (Fig. 3 [Right]). For an inelastic scattering event the nuclear recoil and the electron recoil induced by nuclear de-excitation γ conversion come practically at the same time and share the energy of the incoming neutron: the produced signal is thus a superposition of a gamma-like and a neutron-like signal and is characterized by a F_p value in between that of an electron and nuclear recoil [13]. To validate the origin of this intermediate component and to find the most appropriate fitting function able to reproduce the experimental F_p distributions, a MonteCarlo (MC) simulation was developed to reproduce the energy released in the detector by the interaction of both neutrons and γ particles emitted by the Am/Be source [15]. Neutron interaction cross-sections from the JENDL database [16] were used for the MC event generation and included the elastic and inelastic channels. The results of the simulation confirmed the hypothesis of the intermediate population in the F_p distribution resulting from inelastic neutron scatters; subsequently a fitting function Fit_{tot}, able to reproduce the acquired data, has been found as a sum of two gaussian functions for the neutron and γ populations with the addition of a convolution of a gaussian and an exponential function for the intermediate population:

$$Fit_{Tot} = G_\gamma \oplus G_n \oplus (exp \otimes G)_i \tag{3}$$

In Fig. 4 real [Left] and simulated [Right] overall F_p distributions for events in the energy range $200 < S_1 < 260$ phe with the superimposed fitting function for intermediate events have been shown. The percentage of inelastic events with respect to the neutrons varies with the deposited energy rising from a small contribution to a significant fraction of the number of neutron events at highest energies.

Data belonging to the analysis data sample have been divided into 26 energy bins of variable size: a 5 phe bin width is choosen for event energies $40 < S_1 < 100$ phe, 10 phe bin width for $100 < S_1 < 200$ phe and 15 phe bin width for $200 < S_1 < 260$ phe; thus, the smallest energy interval includes event consisting of $40 \div 45$ phe, while the largest bin including events in the range of $245 \div 260$ phe.

A fit with the Fit_{Tot} function defined in Eq. (3) has been performed for each distribution at every energy bin and $\langle F_p \rangle$ values for the gamma and neutron gaussian populations have been extracted; these are reported in Fig. 6.

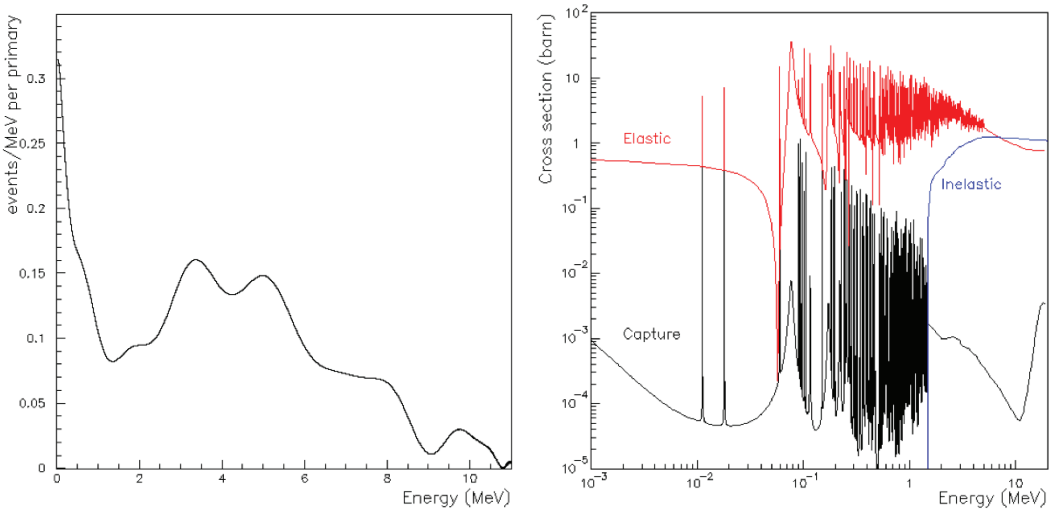

Fig. 3. *Primary neutron spectrum for the Am/Be source [Left] and cross-section for different interactions on the* ^{40}Ar *[Right].*

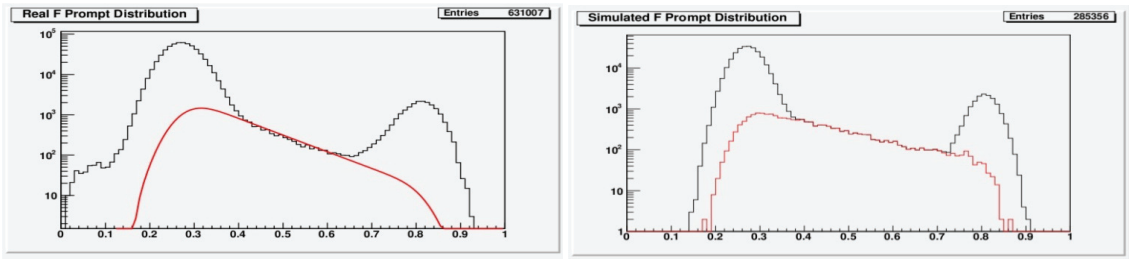

Fig. 4. *Real [Left] and simulated [Right] overall* F_p *distributions for events in the energy range 200*$< S_1 <$*260 phe with the superimposed fitting function for intermediate events.*

5. New measurements at high Light Yield

In order to test the results obtained in the previous test, a new measurement with the same single phase LAr detector (no electric fields), refurbished with four 3" High Quantum Efficiency (HQE) PMTs (Hamamatsu R11065)[4] and a new DAQ system (signals from the 4 PMTs have bee directly acquired by means a new fast waveform digitizer CAEN V1751 [17]), has been performed.
For this test, the chamber was radiated again with an Am/Be source to explore the detector response to neutrons; in addition blank runs and runs with ^{241}Am have been acquired to control the environmental background and to evaluate the detector LY respectively. Compared with the previous test, set-up modifications resulted in obtaining a much higher Light Yield with LY=6.35 phe/keV±5% (to be compared with ∼1.5 phe/keV) [18]. These new detector parameters allowed to test the signal-to-background separation capability obtainable in particular at lower recoil energies improving the sensitivity and the precision of the measurement with the Am/Be source.

5.1. Data analysis of the new test

The data was taken during a short neutron run in February, 2011. For the neutron background separation analysis $20 \cdot 10^6$ Am/Be events were collected including $1.5 \cdot 10^6$ neutron candidate events. The percentage

[4]The second test set-up is equivalent in size and photo-cathode coverage to the first.

of neutron events in the data was approximately twice as high (over 7%) as in the previous measurements (3.5%) [13]. The much higher statistics and the new DAQ system allowed performing background subtraction.

After the basic cuts were applied to the data, the surviving events were divided into 93 energy bins chosen to contain a similar number of entries. This resulted in much wider bins in the upper end of this spectrum. Then, for each bin, the same F_p distribution model (Eq. (3)) established in the first test was fitted. Also in this case the intermediate population was present (Fig. 5 [Right]) (due to the extended dynamic range of the new wfm recorder in use with this test the neutron events were not saturated until over 2000 phe) (Fig. 5 [Left]) [19].

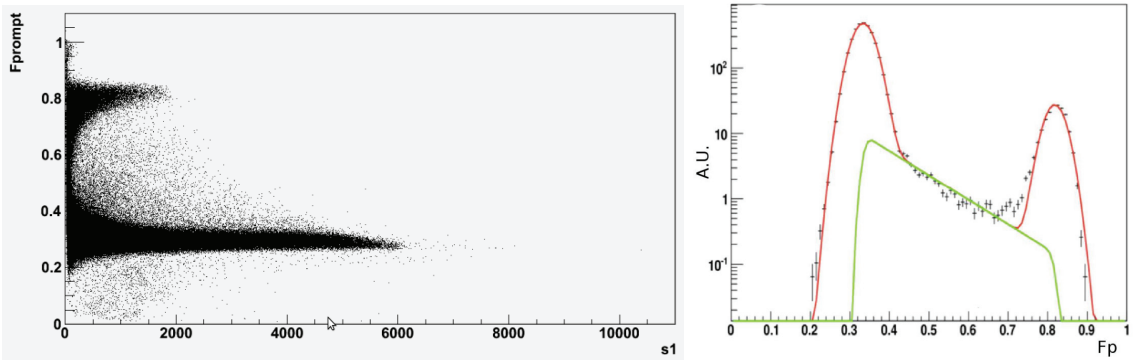

Fig. 5. *The F_p vs S_1 plot with the nuclear/neutron recoils and electron/gamma recoils (full range of the detected energies is shown) [Left]; F-prompt distribution in the interval $545 < S_1 < 560$ phe [Right].*

5.2. Results and comparison of the performed tests

As in the previous measurement, the F_p discrimination technique described above was applied to the analysis data samples acquired during the two tests. The positions of the gamma and neutron peaks for each of the energy bins resulted in mean values of the *F-prompt* parameter $\langle F_p \rangle$ for given energy values.
This allowed plotting the estimated $\langle F_p \rangle$ value both for nuclear recoil-like and electron recoil-like events as a function of the event energy [keV] for both the performed tests, which is presented in Fig. 6. Errors reported are only statistical, defined as the standard deviation obtained, for each energy bin and for each population, from the $\langle F_p \rangle$ values; systematic errors are still under investigation.
It is worth noting that the $\langle F_p \rangle$ values of the gamma and neutron populations become closer with lower energy, implying a worse separation in that region. This effect seems to be independent of the fitting method applied or the integration window of both the signal and its fast components and has in fact been observed by other experimental groups [22].

To compare the results from the two performed tests, they have both been translated into units of energy using the respective Light Yields measured using radioactive gamma emitting sources. For the neutron population an additional correction was applied to the respective Light Yield due to the quenching of scintillation light from nuclear recoils. The quenching factor was assumed to be equal to 0.25 and constant in the whole energy range [21]. A second correction was needed to take into account the different contamination of the liquid Argon used in both measurements. Impurities in liquid Argon, especially O_2 and N_2 can affect the Light Yield, mainly for the slow component [11] [20], which affects the value of the S_1 integral but not that of S_F in Eq. 2 and so would systematically shift the F_p values. Due to a significant N_2 contamination in the second run[5] [18] a corrective factor has been applied to the presented F_p values.

Compared to the first run, data acquired with the new set-up showed a much wider energy range due to the higher Light Yield (in lower energies) and higher full scale range of the new board (higher bins), but

[5]The value of $\tau_T \sim 1100$ ns of the 2011 test to be compared with $\tau_T \simeq 1350$ ns for the 2009 run

also a slightly worse neutron-to-gamma separation. The shifting down of the neutron population could be due to the fact that with the new set-up the optimum integration time for the fast component was found to be shorter (100 ns vs 120 ns) than in the old test.

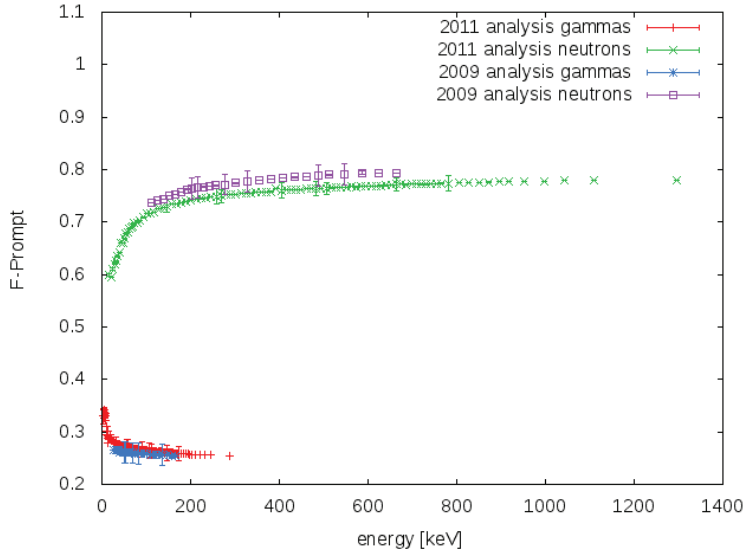

Fig. 6. *F-prompt vs Energy [keV] for neutrons and γ events compared for the two performed tests.*

5.3. Comparison with reference data

The results presented in Fig. (6) from our measurements and analysis can be compared with a reference data set published in 2008 by Lippincott et al. [22].
Those results refer to a detailed PSD study in LAr performed by irradiating with a D-D neutron-generator (E_n=2.8 MeV) a ~3.1 lt LAr cell featuring a Light Yield of 4.85 phe/keV. PSD level has been determined with the *F-prompt* method. Compared to our analysis, the integration time of the fast component in the F_p definition (Eq. 2) was set to a lower value (90 ns instead of 120 ns and 100 ns, as in our first and second test respectively) and the fitting function for the F_p distributions included the sum of two gaussian functions for the neutron and γ populations.
Numerical data from that analysis as reported in [22] are displayed in Fig. 7 together with our results (first and second test) in the full energy range [Left] and with a zoomed view in the low energy interval up to 100 keV_{ee} of recoil energy [Right].

In the range of overlapping energies (Fig. 7 [Right]) the $\langle F_p \rangle$ values for γ's very closely superimpose with each other. Neutron data show instead a systematically higher separation from γ in our data compared to the reference data reported in [22].

A wider n-to-γ separation is of great importance for LAr based detectors as directly reflects in a more extended sensitivity (e.g. in the standard mass vs. cross-section plot in use for WIMP-DM search characterization).

A dedicated study for the identification of possible systematic effects in our measurement is currently under way. It is worth mentioning that applying the same procedure of [22] (same integration time and two gaussian fit function) for the *F-prompt* analysis of our first data set, overlapping results have been obtained for both neutron and γ data. This strengthens our hypothesis of the need to take into account the presence of the intermediate F_p population due to inelastic neutron scattering (becoming relevant at neutron energies in the few MeV range).
Further studies with our second recent data set are on-going and necessary to definitively clarify this issue.

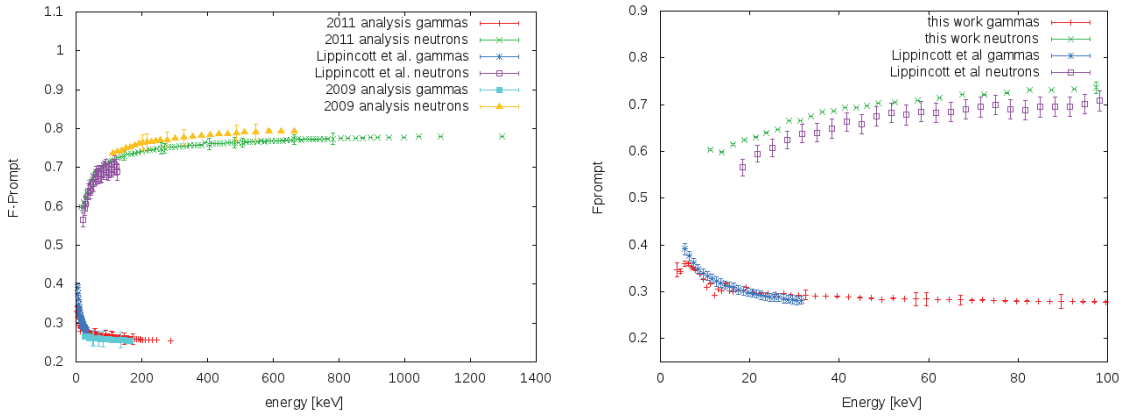

Fig. 7. *The F_p vs Energy [keV] : comparison of the nuclear/neutron recoils and electron/gamma recoils separation power among the two performed tests and data referred to [22] [Left]; comparison between last run and data from [22] at lower energy bins [Right].*

6. Conclusions

Dedicated tests have been performed to estimate the signal to background separation in a single phase Liquid Argon based detector by means of Pulse Shape Discrimination methods. The Argon cell was exposed to an Am/Be source.

In a first run the detector with a rather modest Light Yield of $\sim$ 1.5 phe/keV was used to compare various PSD algorithms; an optimized version of the commonly used *F-prompt* method has been found to be the most efficient.

The optimization required to take into account the presence of a third intermediate population, in addition to those corresponding to neutron and gamma events, in the F_p distribution. We ascribe this type of events to inelastic scattering of neutron on Ar nuclei. The energy spectrum of the Am/Be source and the neutron inelastic cross-section in this range justify this hypothesis. A MonteCarlo simulation of the energy released in the detector by the interaction of neutrons emitted by the Am/Be source further confirms the presence of the intermediate F_p population. To take into account this feature of the *F-prompt* experimental distribution an empirical function to fit the data has been appropriately defined. This in turns allows for a better neutron to gamma separation as a function of the deposited energy.

A second test using the same detector with an increased LY$\sim$ 6.3 phe/keV has been recently performed. The much higher LY during this last run allowed to studying the separation down to very low energies deposited in liquid Argon.

Further dedicated study for the identification of possible systematic effects in our measurement is still under way as well as comparison with other available reference data.

The wider n-to-γ separation extended in the low energy range leads to a better background rejection power. This effect immediately reflects in a higher sensitivity in the direct detection of WIMP-DM particles.

References

[1] C. Rubbia *et al.*,
A programme to search for WIMP particles in Liquid Argon at the LNGS, Letter of intent, Univ. of Pavia, July 1999;
WArP Collaboration,
First results from a dark matter search with liquid Argon at 87 K in the Gran Sasso underground laboratory, Astropart. Phys. **28** (2008), 495.

[2] T. Doke,
Fundamental properties of liquid Argon, Krypton and Xenon as Radiation detector media, Portgal Phys. **12** (1981), 9.

[3] S. Kubota *et al.*,
Recombination luminescence in liquid Ar and Xe, Ph. Rev. B **17** (1978), 2762;
S. Kubota *et al.*,
Dynamical behaviour of free electrons in the recombination process in liquid Ar, Kr and Xe, Phys. Rev. B **20** (1979), 3486.
[4] M. Miyajima *et al.*,
Average energy expended per Ion pair in liquid Argon, Ph. Rev. A **9** (1974), 1438 [and *Erratum*, Ph. Rev. A **10** (1974)].
[5] T. Doke *et al.*,
LET dependence of scintillation yields in liquid Ar, Nucl. Inst. and Meth. A **269** (1988), 291;
T. Doke *et al.*,
Estimation of absolute photon yields in liquid Ar and Xe for relativistic electrons, Nucl. Inst. and Meth. A **291** (1990), 617;
T. Doke *et al.*,
Absolute Scintillation Yelds in Liquid Argon and Xenon for various particles, Jpn. J.Appl.Phys. **41** (2002), 1538.
[6] E. Morikawa *et al.*,
Argon, Krypton an Xenon excimer luminescence: from dilute gas to the condensed phase, J. Chem. Phys. **91** (1989), 1469.
[7] D.E. Groosjean *et al.*,
Absolute luminescence efficiency of Ion-bombarded solid Ar, Ph. Rev. B **56** (1997), 6975.
[8] T. Heindl *et al.*,
The scintillation of liquid Argon, EPL **91** (2010), 62002.
[9] A. Hitachi *et al.*,
Effect of ionization density on the time dependence of luminescence from liquid Ar and Xe, Ph. Rev. B **27** (1983), 5279;
S. Kubota *et al.*,
Variation of scintillation decay in liquid Argon excited by electrons and Alpha particles, Nucl. Inst. and Meth. **150** (1978), 561.
[10] S. Himi *et al.*,
Liquid and Solid Argon, and Nitrogen-doped liquid and solid Argon Scintillators, Nucl. Inst. and Meth. **203** (1982), 153.
[11] R.Acciarri *et al.*,
Effects of Nitrogen contaminations in Liquid Argon, Journal of Instrumentations - 2010 JINST 5 P06003 (2010).
[12] M.J. Carvalho *et al.*,
Luminescence decay in condensed Argon under high energy excitation, J. Lumin.18-19 (1979), 487.
[13] R. Acciarri,
Measurement of the scintillation time spectra and Pulse Shape Discrimination of low-energy electron and nuclear recoils in liquid Argon with the WArP 2.3 lt detector, PhD Thesis, 2010.
[14] J.W. Marsh *et al.*,
High resolution measurements of neutron energy spectra from Am-Be and Am-B neutron sources, Nucl. Inst. and Meth. **366** (1995), 340.
[15] L. Pandola,
MonteCarlo simulation of the WArP-2.3 l detector in the Hall di Montaggio exposed to a AmBe neutron source, WArP Coll. Internal Note, 2009.
MonteCarlo simulation of the measurement with AmBe neutron source for the determination of the Light Yield, WArP Coll. Internal Note, 2006.
Updated evaluation of neutron-induced background in the WArP 100 liter set-up, WArP Coll. Internal Note, 2006.
[16] JENDL Library,
version 3.3, http://wwwndc.tokai.jaeri.go.jp/jendl.
[17] R. Acciarri *et al.*,
Tests of PMT Signal Read-out in a Liquid Argon Dark Matter Detector with a New Fast Waveform Digitizer, arXiv:1203.1371, to be submitted to Jinst-Journal of Instrumentations.
[18] R. Acciarri *et al.*,
Demonstration and comparison of photomultiplier tubes at liquid Argon temperature, Journal of Instrumentations - 2012 JINST 7 P01016 (2012).
[19] P. Kryczynski,
The Effect of Using Isotopically Depleted Argon on Dark Matter Detection Prospects, M. Sc. Thesis, 2011.
[20] R. Acciarri *et al.*,
Oxygen contamination in liquid Argon: combined effects on ionization electron charge and scintillation light, Journal of Instrumentations - 2010 JINST 5 P05003 (2010).
[21] D. Gastler *et al.*,
Measurement of scintillation efficiency for nuclear recoils in liquid Argon, arXiv:1004.0373v2 [physics.ins-det], (2011)
[22] W.H. Lippincott *et al.*,
Scintillation time dependence and pulse shape discrimination in liquid Argon, Phys. Rev. C **78** (2008), 035801